An Add-On Self-Tuning Control System for a UPFC Application

Urvi Malhotra, *Student Member, IEEE*, and Ramakrishna Gokaraju, *Member, IEEE*

***Abstract*—This paper presents an add-on self-tuning (ST) control scheme for a Unified Power Flow Controller (UPFC) to assist its conventional PI control system in damping power oscillations. The ST control algorithm is based on a Pole Shift (PS) technique that has previously been successfully applied in Adaptive Power System Stabilizers (APSSs). For a wide range of operating conditions, the conventional PI-UPFC unless retuned suffers from insufficient/nonoptimal damping performance. To overcome this problem, the authors propose supplementing the PI controllers with an ST feedback loop comprised of an identifier and a PS control algorithm. With a CRLS identifier tracking the system conditions online, this scheme eliminates the need for PI parameter retuning. Further, to correctly identify system parameters during large disturbances, a constrained recursive least squares (CRLS) identification procedure is adopted here. An improved damping performance with the proposed add-on scheme assisting the nonoptimal PI-UPFC is demonstrated for a two-area power system.**

***Index Terms*—Adaptive control, flexible AC transmission systems (FACTS), power systems control, self-tuning (ST) control.**

I. Introduction

AN ever-increasing demand in electricity accompanied with restricted building of new transmission facilities has caused today's interconnected power systems to be overloaded. As a consequence, low frequency (0.1 to 0.8 Hz) inter-area oscillations are often observed when power systems interconnected through weak tie lines are subjected to disturbances such as faults, line outages and sudden load changes. Previously, power system stabilizers (PSS) installed at generator locations were used to damp such system oscillations. However, PSSs are localized stabilizers and hence best suited for damping local oscillatory modes in the power system. Since inter-area modes are related to the dynamics of an inter-connected power system, damping control methodologies meant for transmission paths evolved. The advancements in high-power semiconductors led to the advent of flexible AC transmission systems (FACTS) technology. One such FACTS device—the Unified Power Flow Controller (UPFC), proposed by Gyugyi in 1991 [1]—is a versatile device capable of simultaneously controlling line power flows as well as providing voltage support to the connected bus. In addition to being capable of controlling line power flows, the UPFC can also damp out power oscillations. This has been successfully demonstrated in the past with a suitable UPFC damping control system [2], [3]. A majority of these control systems has employed conventional-PI (or lead-lag) controllers as feedback controllers, providing satisfactory damping performance around a specific operating point. In [4], the FACTS controller design was based on fixed-gain PI controller wherein the controller gains remain fixed during the FACTS device's operation. The tuning of PI controllers is a complex task in a bulk power system involving number of switching devices [5].

PI controllers are fixed-parameter based controllers. The drawback of such PI controllers is that their performance degrades as the system operating conditions change [6]. In [7], a sliding-mode control approach is proposed as a robust controller. However, the controller's performance is dependent on the transfer function, which in the case of a power system modeled with a FACTS device, is difficult to find (to accurately represent the complexity of the system). Furthermore, given the dynamic and nonstationary characteristic of a power system, PI controllers unless retuned cannot ensure consistent damping performance over a wide range of operating conditions. In contrast, artificial neural networks (ANNs) and fuzzy logic have been proposed to adapt the controller gains [8]–[10]. However, such approaches either require offline training or depend on the inference rules. Some of the difficulties associated with the tuning of membership functions in the fuzzy PID type controllers are very well explained in [10].

An artificial immune system (AIS) based modern control approach is proposed in [11] for generator excitation systems to solve the power quality problems, but the design and analysis procedures are complex and difficult. Recently [12] described an adaptive controller for synchronous reluctance motor drives to control the current, speed and position. The adaptive controller in [12] provided good tracking during steady-state conditions and small load disturbance conditions.

The proposed self-tuning (ST) controller in this paper differs from the ANN and Fuzzy Logic control approaches. Unlike ANNs, it does not require offline training nor is dependent on inference rules, which are essential for fuzzy approaches. It instead addresses these deficiencies by exploiting the principles of indirect adaptive control theory. Indirect adaptive control principle consists of an identifier and controller. The identifier works on an estimated plant model of a power system; an auto-regressive moving average (ARMA) model. It identifies the ARMA parameters online and uses parameter estimates to adaptively tune the corresponding control parameters thereby

Manuscript received July 9, 2012; revised February 16, 2013; accepted May 7, 2013. Date of publication July 9, 2013; date of current version October 18, 2013. This work was completed at the University of Saskatchewan as part of the M.Sc. thesis research work of U. Malhotra. The work of R. Gokaraju was supported by an NSERC Discovery Grant.

U. Malhotra is with the Saskatchewan Power Corporation in Regina, SK S4P 0S1, Canada.

R. Gokaraju is with the University of Saskatchewan, Saskatoon, SK S7N 5A5, Canada (e-mail: rama.krishna@usask.ca).

Color versions of one or more of the figures in this paper are available online at http://ieeexplore.ieee.org.

Digital Object Identifier 10.1109/TIE.2013.2272272

yielding a satisfactory control performance. The adaptive identifier and controller described works well for large disturbances as well.

The proposed ST controller consists of an adaptive constrained recursive least squares (CRLS) identifier and a pole shift (PS) controller. The PS controller is self-tuning type, which means that it adapts to the power system conditions online. The self-tuning control technique based on PS control logic was previously implemented on APSSs and certain FACTS devices [13]–[15], however this is the first time it is being developed for a UPFC.

The performance of the proposed ST control scheme depends on accurate determination of the ARMA parameters. It was previously reported in [16] that an RLS identifier at the start of the estimation process gives poor estimation results due to large initial transients present in the system. Such rapid parameter fluctuations result in the ringing of the controller output. If the control is generated on the basis of these highly varying estimated coefficients of the ARMA model, it can lead to unwanted initial power swings in the power system.

To achieve parameter tracking, [16] proposes the use of regularized constant trace algorithm on a Kalman filter identifier. The authors also use a larger 12th order autoregressive (AR) model to capture the system dynamics.

Reference [15] proposes a random walk (RW) method for the RLS identifier for better parameter tracking. The RW algorithm is enabled for a specified duration following a large disturbance to obtain smoother variations in the identified coefficients. A dead-zone is also created for the controller to give time for the RW identifier to estimate the parameters. Furthermore, the authors use a large 10th order ARMA model for the plant and a fixed pole-placement method to generate the control signal.

For self-tuning control, it is important to keep the computation time low. A higher order model (10th or 12th model) means more calculations for the identifier and the controller. Therefore, using a reduced order model, which can capture the essential dynamics, was one of the objectives of this paper.

In this paper, a simple third-order ARMA model is proposed to represent the dynamic oscillations in the power system and it has been found to be sufficient to represent the low frequency power oscillations in the power system. This is because a third-order model has three poles: a pair of complex poles and a real pole. The complex poles represent the oscillatory behavior of the power oscillations and could be used to damp the overshoot using the PS controller; whereas the real root represents the decaying part of the oscillatory response and could be controlled with the PS controller to achieve the desired steady-state response.

This paper also proposes a computationally efficient modification to the standard RLS identifier known as constrained-RLS (CRLS identifier) discussed in Section III-A. The method is simple and involves only a minor calculation step. The CRLS identifier smooths out parameter variations efficiently during large disturbances (i.e., large power swings) following a fault condition. Using the proposed approach, there is no need to create a control dead-zone but instead the controller and identifier are allowed to function all throughout the disturbance condition in unison. It also implies that with the CRLS identifier, the controller is able to adapt to drastic or sudden disturbances in the power system configuration and still ensure a stabilizing control performance.

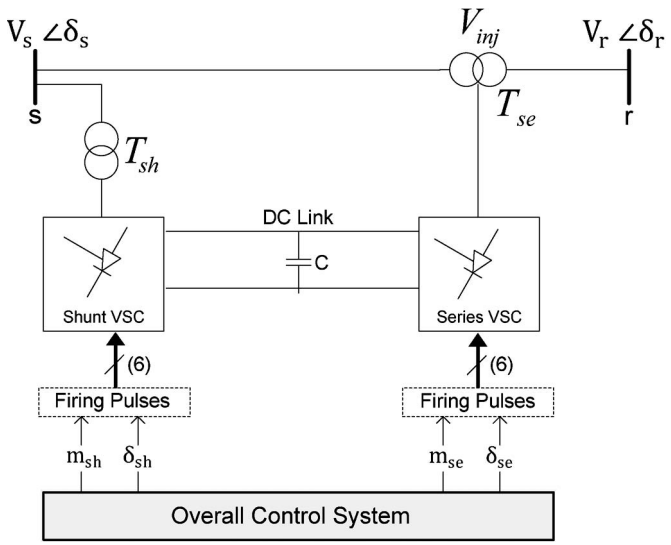

Fig. 1. Single line diagram of a UPFC installed in a two-area power system.

The main contributions of this work are: 1) An adaptive add-on control scheme is proposed on top of a PI-control loop. The scheme retains the functionality of the existing PI controllers while improving the overall damping performance with an add-on supplementary self-tuning control loop. It is worth noting here that the previous literature cited the inability of the self-tuning controllers to handle large disturbance conditions. 2) Use of a constrained-RLS identifier instead of the classical RLS identifier to smoothly track system parameters during large disturbances. The CRLS identifier prevents ringing of the control output during initial post-fault power swings thereby eliminating the need to disable the control action right after a fault occurs.

The paper is organized as follows: Section II discusses the UPFC operation and control system model. A brief discussion of the proposed ST control scheme is presented in Section III. The proposed overall UPFC control system is applied to a multi-area test system and the results are presented in Section IV; Section V reports the conclusions of this work.

II. UPFC: Operation and Control System Model

Fig. 1 shows a schematic representation of a UPFC installed at the sending-end bus, s that serves as an inter-tie of a two-area transmission network. In the past, a majority of literature such as the ones described in [1], [2] have modeled the UPFC as a series reactance with a set of active and reactive nodal power injections or by two ideal voltage sources. Such models were primarily chosen for their mathematical simplicity where the converter switching characteristics were ignored. However, it is important to include the switching characteristics especially when studying the interaction of the converters and the power system in response to system faults. Thus, in this work the UPFC converter is modeled in PSCAD-EMTDC using a two-level, six-pulse voltage sourced converter (VSC) topology

with the thyristor firing pulses generated through a pulse width modulation (PWM) switching technique.

A. Operation

A UPFC consists of two identical converters, the shunt VSC and the series VSC connected in shunt and series with the ac transmission network, respectively. Each converter is connected to the ac system through corresponding coupling transformers, T_{sh} and T_{se} and are operated from a common dc link supported by a dc capacitor, C.

In general, the operation of a UPFC is governed by its four control inputs: $m_{sh}, \delta_{sh}, m_{se}, \delta_{se}$ that are governed by firing commands given to its thyristors switches where m and δ denote converter modulation index and phase angle, respectively. The primary function of the UPFC is provided by the series VSC that generates a voltage $V_{inj}(t) = |V_{inj}| \sin(\omega t - \varnothing_{inj})$ at fundamental frequency (ω) with variable amplitude $(0 \leq |V_{inj}| \leq |V_{inj}|_{\max})$ and phase angle $(0 \leq \varnothing_{inj} \leq 2\pi)$ that is added to the ac system by the series coupling transformer, T_{se}. On the other hand, the shunt VSC serves two purposes. It primarily provides the real power demanded by the series VSC from the ac system via the common dc link. This is made possible by keeping the dc link capacitor, C charged at all times, replicating an energy source for real power exchange. It also acts as an independent reactive power compensator thereby maintaining the system bus voltage at a specified value. With its four control inputs, the UPFC can be commanded to force an appropriately varying line power to effectively damp power oscillations.

B. Damping Control

The control of a UPFC can be divided into two parts—the control of the shunt VSC and the series VSC where each VSC is controlled by two control inputs—modulation index, m and phase angle, δ. The shunt and series VSCs can be operated in different control modes [1] where a particular mode is chosen depending upon the application objective. For damping of inter-tie oscillations, the series VSC is operated in *Automatic Power Flow Control* mode as shown in Fig. 2(a). The d-q control method suggested in [17] is adopted wherein the desired $P_{desired}$ and $Q_{desired}$ are compared with the measured line flows, P_{meas} and Q_{meas} and the corresponding deviations in real and reactive power (ΔP and ΔQ) are used to drive the d-q components (V_d and V_q) of series injected voltage, V_{inj}. Note here that m_{se}, m_{sh} and δ_{se}, δ_{sh} correspond to steady-state converter settings that can be easily obtained depending upon the desired inter-tie real and reactive power flows.

For the purpose of tightly regulating the connected bus voltage ($< 5\%$), the shunt VSC is operated in *Automatic Voltage Control* mode as shown in Fig. 2(b). The bus voltage regulation is accomplished by varying the shunt modulation index, m_{sh} while the dc link voltage regulation is achieved by varying the phase angle order, δ_{sh}.

The UPFC control of Fig. 2 is based on PI control law that is inadequate in tracking the system changes and become increasingly less effective in damping power oscillations with a set of non-optimal PI parameters. On the contrary, the proposed ST controller copes to system changes and offers an excellent tracking capability even for large disturbances such as three-phase faults. Further, in a UPFC the series VSC can directly influence the power flow and hence the oscillatory modes. Keeping the aforementioned points in mind, the proposed ST controller is added as a supplementary control loop to the series VSC to modulate m_{se} as shown in Fig. 2(a) with the real power deviations, ΔP as the control input.

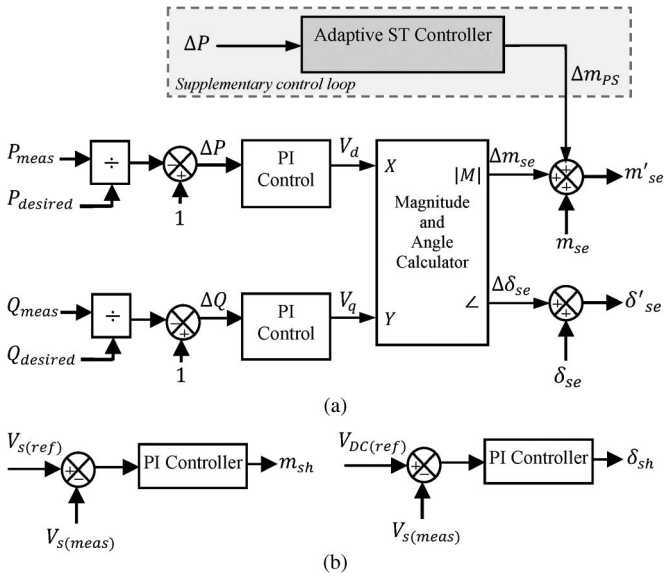

Fig. 2. Overall UPFC control system for a damping application. (a) Series VSC control system; (b) Shunt VSC control system.

III. Self-Tuning (ST) Controller

The major drawback of the UPFC control system discussed in Section II is that it is solely based on PI controllers. As mentioned before, PI controllers create the need for frequent tuning and hence are inefficient in damping power oscillations under different operating conditions. On the contrary, the proposed ST controller being adaptive is independent of tuning. With the ST controller in the feedback loop, it is expected to significantly improve the damping capability offered by the overall UPFC control system.

Fig. 3 represents the schematic overview of the ST controller. Note that here the measured output $y(t)$ from the power system is the oscillations in real power ΔP while the controller output $u(t)$ is the damping input Δm_{se} supplied to the series VSC of the UPFC.

A. System Estimation: Adaptive CRLS Identifier

Amongst several identification algorithms used for online parameter estimation, the classical recursive least squares (RLS) method has the advantage of simple calculation and good convergence properties [18]. The algorithm assumes the process (here, power system including the UPFC) to be described by a discrete ARMA model of the form

$$A(z^{-1})y(t) = B(z^{-1})u(t) + e(t) \tag{1}$$

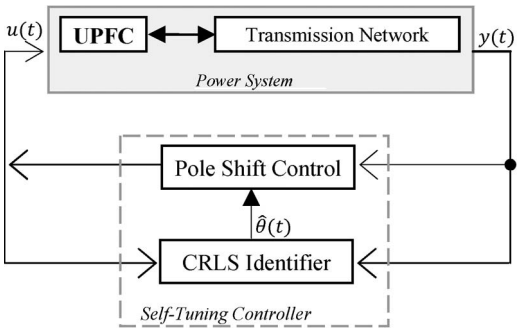

Fig. 3. Self-tuning (ST) control.

where $A(z^{-1})$ and $B(z^{-1})$ are polynomials in backward shift operator z^{-1} and are defined as

$$A(z^{-1}) = 1 + a_1 z^{-1} + a_2 z^{-2} + \dots a_{n_a} z^{-n_a}$$
$$B(z^{-1}) = b_1 z^{-1} + b_2 z^{-2} + \dots b_{n_b} z^{-n_b}$$

n_a and n_b are the orders of the polynomials $A(z^{-1})$ and $B(z^{-1})$ and variables $y(t)$, $u(t)$ and $e(t)$ are the system output, system input and white noise, respectively. Equation (1) can be re-written in a form suitable for identification as

$$y(t) = \hat{\theta}^T(t)\varphi(t) + e(t) \tag{2}$$
$$y(t) = \hat{y}(t|\hat{\theta}, \varphi) + e(t) \tag{3}$$

where $\hat{y}(t|\hat{\theta}, \varphi)$ is the prediction of $y(t)$ based on estimated system parameter vector, $\hat{\theta}^T(t)$ and measurement variable vector, $\varphi(t)$ defined as

$$\hat{\theta}(t) = [a_1\ a_2\ a_3\ \dots\ a_{n_a}\ b_1\ b_2\ b_3\ \dots\ b_{n_b}]^T \tag{4}$$
$$\varphi^T(t) = [-y(t-1) - y(t-2) \dots - y(t-n_\mathrm{a}) \times u(t-1) \dots u(t-n_\mathrm{b})] \tag{5}$$

where $\varphi^T(t)$ denotes the data vector storing the last n_a samples of the system output and the last n_b samples of the system input. The prediction error, $\varepsilon(t)$ is given by

$$\varepsilon(t) = y(t) - \hat{y}(t|\hat{\theta}, \varphi) = e(t). \tag{6}$$

The RLS criterion determines the most likely value of $\hat{\theta}(t)$ that minimizes the sum of the squares of the prediction error

$$J(N) = \frac{1}{N} \sum_{k=1}^{k=N} [e(t)]^2 . \tag{7}$$

The system parameter vector $\hat{\theta}(t)$ can be calculated by the following set of recursive equations:

$$\hat{\theta}(t) = \hat{\theta}(t-1) + K(t) \left[y(t) - \hat{\theta}^T(t-1)\varphi(t) \right] \tag{8a}$$

where the weighing factor for the last identified parameters is equal to one and that for the prediction error is given by the modification coefficients (or gain matrix) $K(t)$

$$K(t) = \frac{P(t-1)\varphi(t)}{\rho(t) + \varphi^T(t)P(t-1)\varphi(t)} \tag{8b}$$
$$P(t) = \frac{1}{\rho(t)} \left[1 - K^T(t)\varphi(t) \right] P(t-1) \tag{8c}$$

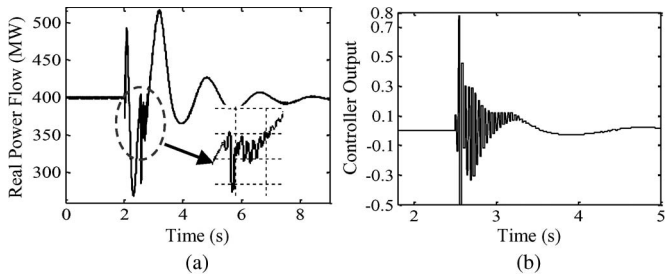

Fig. 4. Excursions in system response following a three-phase fault.

where $\rho(t)$ is the time varying forgetting factor, $P(t)$ is the covariance (of error in estimate) matrix, and $K(t)$ is the gain vector. The forgetting factor $\rho(t)$ is calculated as

$$\rho(t) = \rho_0 \rho(t-1) + (1 - \rho_0); \quad 0 < \rho_0 < 1. \tag{8d}$$

In every iteration, the RLS algorithm uses a set of old and new system measurements to predict the system output $\hat{y}(t)$ and calculate the prediction error $\varepsilon(t)$. Based on $\varepsilon(t)$ and the past history of measurements stored in error covariance matrix $P(t-1)$, it then calculates a set of modification coefficients $K(t)$. Using $K(t)$ it arrives at a new set of identified system parameters $\hat{\theta}(t)$ as in (8a). At the end of the current iteration the information of the new measurements are stored for their use in the next sample. However, if a classical RLS identifier is extended to a power system imposed by large disturbances (faults), it experiences undesired rapid parameter fluctuations. Fig. 4(a) illustrates as an example, a noisy type first-swing inter-area power flow and corresponding ringing of control output [Fig. 4(b)] recorded when a three-phase-ground fault was applied to the neighboring area.

The skewed response is due to the imperfections of the RLS algorithm as it is meant for a system with constant or slow varying parameters [18]. To overcome this drawback, a constrained-RLS (CRLS) identification technique is used that modifies (8a) with the inclusion of a constraint term $\beta(t)$

$$\hat{\theta}(t) = \hat{\theta}(t-1) + K(t) \left[y(t) - \hat{\theta}^T(t-1)\varphi(t) \right] \beta(t) \tag{9}$$

where $\beta(t)$ is calculated at each sampling instant as follows:

$$\beta(t) = \begin{cases} 1.0 & \text{if } \frac{N_2}{N_1} \le \beta_0 \\ \frac{\beta_0}{N_2} & \text{if } \frac{N_2}{N_1} > \beta_0 \end{cases} \tag{10}$$

where

$$N_1 = \left\| \hat{\theta}(t) \right\|_2$$
$$N_2 = \left\| K(t) \left[y(t) - \hat{\theta}^T(t-1)\varphi(t) \right] \right\|_2$$

$\|.\|_2$ is the norm of the corresponding vector and β_0 is a positive constant which determines the rate of parameter update. At the time of fault inception (and the duration shortly after) on a power system, the ratio N_2/N_1 progresses quickly to be greater than β_0. During this time period $\beta(t)$ takes the value β_0/N_2 reducing the estimation rate and therefore contributing to a smooth controller action. After fault removal when the power system is moving to a stable operating point, the ratio N_2/N_1

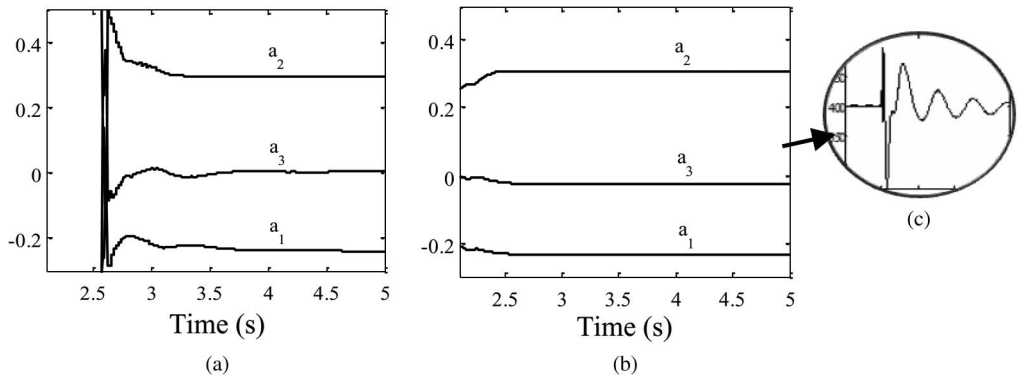

Fig. 5. Excursions in a-parameters following a three-phase fault. (a) a-parameters with RLS identifier; (b) a-parameters with CRLS identifier.

gradually progresses to be less than β_0 making $\beta(t) = 1$. At this time, the constrained-RLS algorithm automatically switches back to the standard-RLS algorithm. It is worth noting that a larger β_0(i.e., $\beta_0 > 0.75$) slows down the estimation rate which is undesirable; while choosing a smaller β_0(i.e., $\beta_0 < 0.5$) can cause the identifier to respond to even minor disturbances. Therefore, $\beta(t)$ is chosen as 0.5 to achieve optimal tracking capability. The $\beta(t)$ in (9) initiates a smooth controller response a scan be seen in Fig. 5. Fig. 5 gives a plot of varying a-parameters versus time for the example illustrated in Fig. 4. The minimization of drastic parameter variation by the CRLS identifier and its successful application to a faulted power system is evident from the power flow response shown in Fig. 5(c) as opposed to the power flow response of Fig. 4(a).

It should be pointed out that for all the studies using the ST controller, a third-order ARMA system model is used in the identification process. When a two-area system is subject to a disturbance it exhibits inter-area mode of oscillations in the range of 0.1 to 0.8 Hz, and a third-order model has been found to be sufficient to represent this single mode of oscillation as discussed in the introduction.

A second-order model is not useful because it can only represent either the oscillatory (pair of complex conjugate poles) or the non-oscillatory part (with real poles). With a 4th order model, the system could be identified as two pairs of complex conjugate poles, or one pair of complex poles and two real poles, or four real poles. Two pairs of complex poles can only represent the oscillatory response, whereas two or four real-poles are not needed to represent the non-oscillatory part of a single mode inter-area oscillation.

A 5th, 7th, 9th or higher odd numbered models could be used. The 5th order, 7th and 9th order models were tried but there was no noticeable damping improvement compared to a 3rd order model. Therefore, 3rd order model was chosen to keep the number of computations less for hardware implementation.

B. Control Algorithm: Pole Shift Control

Once the system parameters are identified by the CRLS identifier, the control signal is calculated based on the discrete system model of (1) by assuming the transfer function of the feedback loop is of the form

$$\frac{u(t)}{y(t)} = -\frac{G(z^{-1})}{F(z^{-1})} \tag{11}$$

where

$$F(z^{-1}) = 1 + f_1 z^{-1} + f_2 z^{-2} + \dots f_{n_f} z^{-n_f}$$
$$G(z^{-1}) = g_0 + g_1 z^{-1} + g_2 z^{-2} + \dots g_{n_g} z^{-n_g}$$

and $n_f = n_b - 1$, $n_g = n_a - 1$. The concept of the PS control is discussed in detail in [13], [14]. It is based on the minimum variance (MV) control and the pole assignment (PA) control. However, unlike the PA method where the closed-loop poles are assigned to specific locations, in the PS method the closed-loop poles are shifted radially toward the center of the unit circle in z-domain by a factor, α (less than one)

$$T(z^{-1}) = A(z^{-1})F(z^{-1}) + B(z^{-1})G(z^{-1}). \tag{12}$$

The characteristic equation of (12) of the closed-loop system takes the form of characteristic equation $A(z^{-1})$ of the open-loop system with the pole shifted by a scalar factor α. Thus (10) takes the form

$$T(z^{-1}) = A(z^{-1})F(z^{-1}) + B(z^{-1})G(z^{-1}) = A(\alpha z^{-1}). \tag{13}$$

Rearranging (13) in matrix form in terms of control parameters $\{f\}$ and $\{g\}$ gives

$$\begin{bmatrix} 1 & 0 & \cdot & 0 & b_1 & 0 & \cdot & 0 \\ a_1 & 1 & \cdot & 0 & b_2 & b_1 & \cdot & 0 \\ \cdot & a_1 & \cdot & \cdot & \cdot & b_2 & \cdot & \cdot \\ a_{n_a} & a_{n_a-1} & \cdot & 1 & b_{n_b} & b_{n_b-1} & \cdot & b_1 \\ 0 & a_{n_a} & \cdot & a_1 & 0 & b_{n_b} & \cdot & b_2 \\ 0 & 0 & \cdot & a_2 & 0 & 0 & \cdot & b_3 \\ \cdot & \cdot & \cdot & \cdot & \cdot & \cdot & \cdot & \cdot \\ 0 & 0 & \cdot & a_{n_a} & 0 & 0 & \cdot & b_{n_b} \end{bmatrix} \begin{bmatrix} f_1 \\ \cdot \\ \cdot \\ f_{n_f} \\ g_0 \\ \cdot \\ \cdot \\ g_{n_g} \end{bmatrix}$$
$$= \begin{bmatrix} (\alpha - 1)a_1 \\ (\alpha^2 - 1)a_2 \\ \cdot \\ \cdot \\ (\alpha^{n_a} - 1)a_{n_a} \\ 0 \\ \cdot \\ 0 \end{bmatrix}$$

or

$$M \cdot \omega(\alpha) = L(\alpha) \tag{14}$$

where the elements of matrix M are the parameters $\{a\}, \{b\}$ that are identified by the identifier every sampling period. If the value of pole shift factor, α, is known, (14) can be solved for the control parameters $\{f\}$ and $\{g\}$ following which control output, $u(t)$ can be obtained using (11). It can be observed that the control signal is a function of α at any time t denoted as α_t. The control signal, $u(t, \alpha_t)$ can be expressed in a Taylor series of factor α_t at a particular point α_0 as

$$u(t, \alpha_t) = u(t, \alpha_0) + \sum_{i=1}^{\infty} \frac{1}{i!} \left[\frac{\partial^{(i)} u(t, \alpha_t)}{\partial \alpha_t^{(i)}} \right] (\alpha_t - \alpha_0)^i. \tag{15}$$

From (11) and (14), the control signal can be expressed as

$$u(t, \alpha_t) = X^T(t)\omega(\alpha_t) = X^T(t)M^{-1}L(\alpha_t) \tag{16}$$

where $X(t) = [-u(t-1).. - u(t-n_f) - y(t) - y(t-1).. - y(t-n_g]^T$ is the measurement variable vecor. The ith order differential of $u(t, \alpha_t)$ with respect to α_t becomes

$$\left[\frac{\partial^{(i)} u(t, \alpha_t)}{\partial \alpha_t^{(i)}} \right]_{\alpha_t = \alpha_0} = X^T(t)M^{-1}L^{(i)}(\alpha_0) \tag{17}$$

where i represents the order of the differentiation. Now (15) can be expressed as

$$u(t, \alpha_t) = u(t, \alpha_0) + \sum_{i=1}^{n_a} s_i \alpha_t^i \tag{18}$$

where $s_i = (1/i!)X^T(t)M^{-1}L^{(i)}(\alpha_0)$.

Once the input is computed at time t, the system predicted output $\hat{y}(t+1)$ at time $t+1$ can be calculated as follows:

$$\hat{y}(t+1) = X^T(t)\mu + b_1 [u(t, \alpha_t)] \tag{19}$$

where $\mu = [-b_2 \ -b_3 \ \cdots \ -b_{n_b} \ a_1 \ a_2 \ \cdots \ a_{n_a}]$ is the identified parameter vector.

The essence of PS algorithm is based on α. The PS factor α is calculated iteratively so as to minimize the one time-step ahead prediction error in system output $y(t)$ given as

$$\underbrace{\min}_{\alpha_t} J(t+1, \alpha_t) = E [\hat{y}(t+1) - y_r(t+1)]^2 \tag{20}$$

where $J(t+1, \alpha_t)$ defines the performance index, E is the expectation operator, $\hat{y}(t+1)$ is next time-step predicted output and $y_r(t+1)$ is the next time-step reference output. The minimization function in (20) is a constrained optimization routine subjected to a stability and control constraint. The stability constraint restricts α_t to be within $((-1/\lambda), (1/\lambda))$ to ensure closed-loop stability at all times, where λ represents the absolute value of the largest root of $T(z^{-1})$. Further, the control constraint emphasizes control signal $u(t, \alpha_t)$ to satisfy $u_{\min} \leq u(t, \alpha_t) \leq u_{\max}$, where $u_{\min}$ and $u_{\max}$ are the minimum and maximum control signal boundaries, respectively. In a UPFC application where the PS control signal modulates m_{se} by a supplementary control loop, $m_{se} is \leq 1.0$ to prevent overmodulation of the series-VSC.

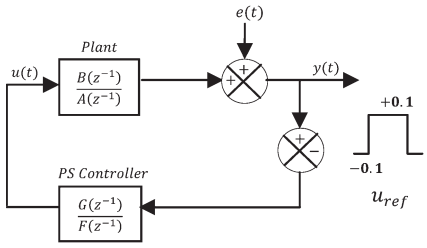

Fig. 6. SISO discrete system with PS controller in feedback loop.

C. ST Controller on Discrete Test System

The performance of the ST control scheme with the proposed CRLS identifier is first investigated on a single input single output (SISO) discrete system as shown in Fig. 6. The plant is an unstable third-order model. During the test, the reference input, u_{ref} is changed every 1 s to assess the performance of the ST controller. That is, to excite the plant for identification and control process, a step-input limited to ± 0.1 $units$ is simulated. The term $e(t)$ in Fig. 6 represents addition of white noise of magnitude 1% to the system.

The discrete system is of the form

$$\begin{aligned} &y(t) - 2.54y(t-1) + 2.69y(t-2) - 1.05y(t-3) \\ &\quad = 0.5u(t-1) + 0.1u(t-2) + 0.25u(t-3) + e(t) \end{aligned} \tag{21}$$

that corresponds to a plant model of

$$\frac{B(z^{-1})}{A(z^{-1})} = \frac{0.5z^{-1} + 0.1z^{-2} + 0.25z^{-3}}{1 - 2.54z^{-1} + 2.69z^{-2} - 1.05z^{-3}}. \tag{22}$$

The open loop plant poles are at -0.82 and $0.86 \pm j0.74$. Thus, the complex conjugate poles of the open loop system are located outside the unit circle and poses the need for a stabilizing feedback signal, $u(t)$. With the PS controller in the feedback loop (Fig. 6) the control signal is calculated using (18) based on the identified plant coefficients using the CRLS identifier of (9). It is worth noting here that although the plant coefficients are defined in (22) they appear *unknown* to the identifier. For this test, convergence of the identified parameters to the *actual* parameters of (22) will essentially demonstrate the success of the identifier. The time-domain system response reference input u_{ref} is plotted in Fig. 7. As can be inferred, the controlled plant is able to track the reference signal effectively. Further, the corresponding identified plant coefficients by the CRLS identifier are plotted in Fig. 7(c) and (d). The CRLS identification not only converges quickly but also provides a smooth parameter tracking during input switching instances. The controller was able to perform satisfactorily even during switching instants due to the CRLS identifier.

Furthermore, the closed-loop stability as ensured by the PS control algorithm can be confirmed with the location of the open and closed loop poles as illustrated in Fig. 8. Open loop poles are shown by "*" while closed loop poles are shown by "x". The identified open loop poles are at $\{0.7437, 0.7988 \pm j0.7203\}$ and the closed loop poles are at $\{0.4821, 0.5083 \pm j0.501\}$ indicating the evidence of radial pole-shifting process by the pole-shift factor α to achieve closed loop stability along with a desired system response.

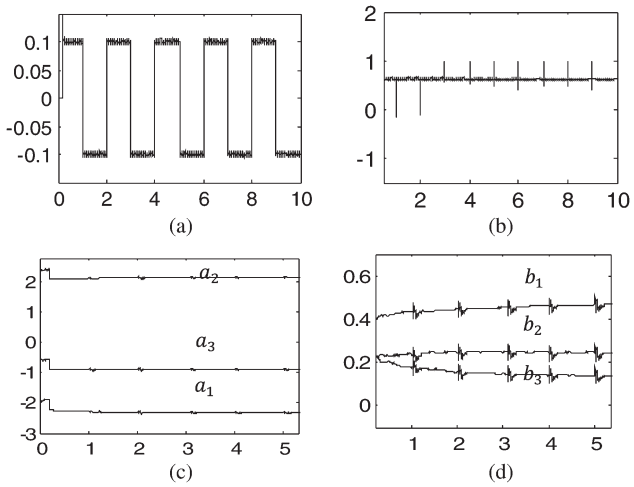

Fig. 7. System time response to step changes in reference input. (a) Plant output; (b) pole shift factor α; (c) plant parameter a; (d) plant parameter b.

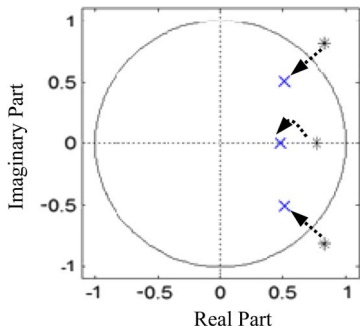

Fig. 8. Dynamic pole-shifting by pole-shift factor α.

IV. Simulation Results

The proposed ST controller is introduced as an add-on scheme to the existing PI UPFC control system. The objective of this paper is to test the damping enhancement capability of the ST controller operating in unison with the non-optimal PI controllers. Kundur's two-area four-machine test system [1] of Fig. 9 investigated by researchers for inter-area mode analysis has been chosen for the study. The system loading is such that net power is exported from *Area 1* to *Area 2*. Three oscillatory modes are present in this system; two intra-area modes (1.04 and 1.13 Hz), one in each area and one inter-area mode (0.52 Hz) where damping of the inter-area mode is of prime concern. To improve the inter-area mode damping, a UPFC is installed on one of the tie-line connecting buses 7 and 8 (sending-end of *Area 1*). The UPFC is equipped with the proposed supplementary ST controller (Fig. 9) to damp power oscillations with real power deviation from bus 7 as the feedback signal.

A. Time-Domain Analysis

The electromagnetic transient simulation software PSCAD/EMTDC is used for simulations. The synchronous generators of Fig. 9 are represented in the $d-q-0$ reference frame by detailed 7th order differential equations, transmission lines are modeled as lumped impedances and system loads as constant impedances. The dynamics of the synchronous machine exciters and governors are also included in the simulations with their details along with the system, UPFC and PI parameters given in Appendix.

Several fault types imposed at four different operating conditions as listed in Table I were studied. Note here that P_{78} refers to the inter-area line power flow with UPFC at the sending end. The UPFC PI parameters were optimized using multiple time-domain simulation based simplex algorithm [19] at operating condition II of Table I. A sampling time of 20 ms (50 Hz) chosen for the adaptive controller was found to be adequate for damping low-frequency (0.1–0.8 Hz) oscillations. Fig. 10 compares the inter-area power flow response between the PI control and the PI control assisted with ST control for a 6 cycle, 3-phase fault (Type A) applied at bus 8. The effectiveness of ST control is evident with the effective damping of power oscillations by the add-on controller as opposed to the standalone-PI controllers. The corresponding series modulation indices (Δm_{se-PI} and Δm_{se-PS}) responsible for providing damped power oscillations on tie-line 7–8 are shown in Fig. 11 where the steady-state value (m_{se}) is 0.475. It can be easily seen that the proposed ST scheme greatly impacts power flow and hence power oscillation damping through larger variations in m_{se}. The ST control signal $u(t)$ under the control limits of ± 0.55 and the varying pole-shift factor α are plotted in Fig. 12.

The behavior of α at post fault occurrence is such that it progresses to a lower value of $\alpha = 0.6025$ indicating maximum control effort and slowly settles at $\alpha = 1.0$ once the subsequent oscillatory swings are adequately damped out. Also, during fault the shunt VSC maintains the shunt bus voltage fluctuation $|\Delta V_7|$ within 0.05 p.u. along with regulating the dc link voltage ($V_{DC(ref)} = 42.4$ kV for all test cases) that facilitates real power exchange between the two VSCs as shown in Fig. 13(a) and (b). Further, the RLS identifier equipped with the tracking constraint $\beta(t)$ of (10) offers a smooth parameter tracking ability even during a large disturbance as shown in Fig. 14.

On the other hand, the improved power oscillation damping of Fig. 10 due to the supplementary pole-shift algorithm can be verified from the corresponding pole-zero plot (in z-plane) of Fig. 15. The open-loop and closed loop poles are plotted as a function of α and their movement is captured from 2 s to 5 s. This snapshot is taken at $t = 2.56$ s when a pole-shift factor of $\alpha = 0.485$ shifted the open-loop poles indicated by a "*" radially inwards to the closed-loop pole locations shown by a "x". Thus the post-fault condition imposed a significant pole-shifting process. For the same power condition, a disturbance of Type B is simulated with the system response (tie-line power P_{78}) and the corresponding pole-shift factor α shown in Fig. 16.

The robustness of the proposed add-on ST controller in damping power system oscillations is validated (Figs. 17–20) for different inter-area power flows and system configurations highlighted in Table I. Fig. 17 depicts a comparison of power flow responses with and without the ST controller in the supplementary loop when the transmission network is subjected to a Type C disturbance. From the responses, it can be ascertained that the oscillations are damped very quickly by the supplementary controller proving its superiority over the conventional PI-UPFC control system.

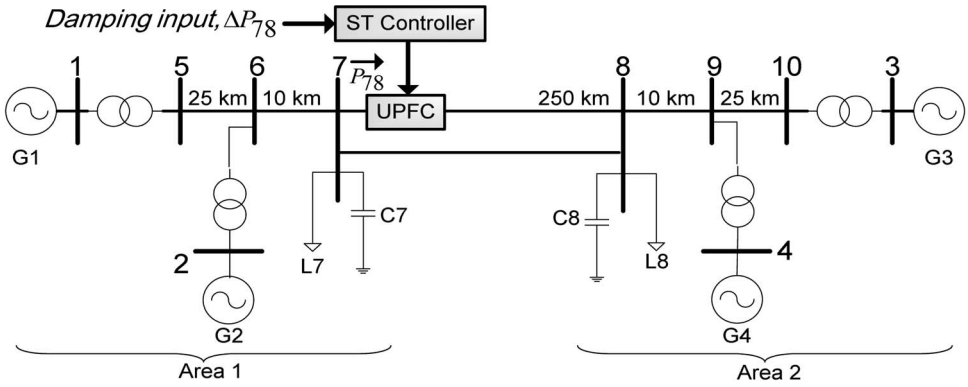

Fig. 9. Two-area power system with UPFC at the sending-end of Area 1.

TABLE I
INTER-AREA OSCILLATION DAMPING CASE STUDIES

Operating Condition	Inter-tie power transfer P_{78}(MW)	Tie length/Tie line (km)	Disturbance description	Disturbance type
I	400	500	4 cycle, 3-phase-ground to fault at bus 8	**Type A**
			6 cycles, 2-phase fault at bus 7	**Type B**
II	300	500	4 cycle, 1-phase-ground fault at bus 8	**Type C**
			8 cycle, 3-phase-ground fault, center of 7-8	**Type D**
III	210	800	3 cycle, 1-phase-ground fault at bus 7	**Type E**
			4 cycle, phase-phase fault at center of 7-8	**Type F**
IV	278	600	Other tie-line disconnected for 64 ms	**Type G**

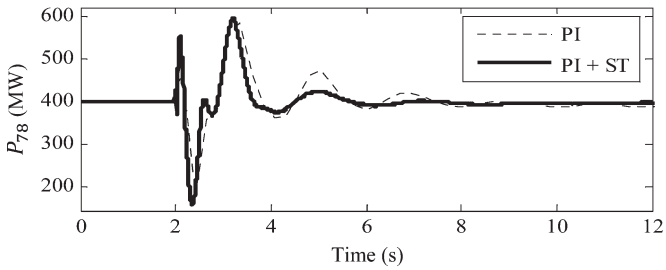

Fig. 10. Tie-line power flow response to a Type A disturbance.

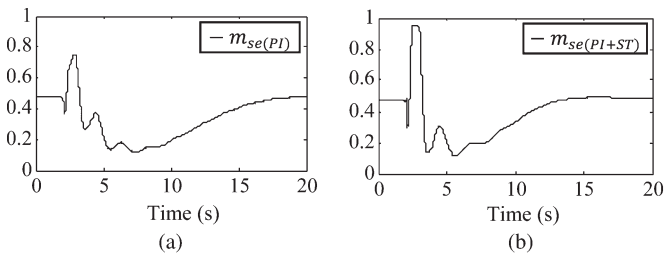

Fig. 11. Overall modulation of m_{se} for Type A disturbance.

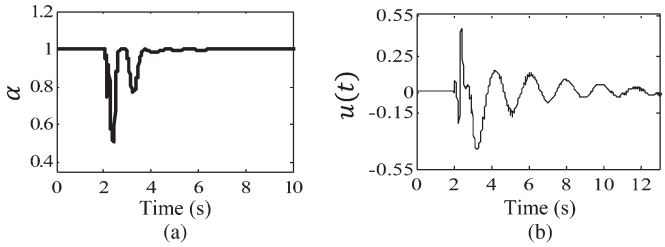

Fig. 12. ST controller output for a Type A disturbance.

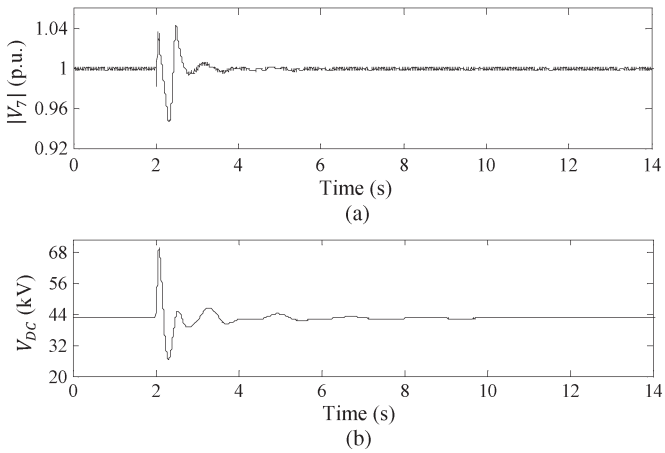

Fig. 13. Shunt bus voltage and dc link voltage regulation by shunt VSC.

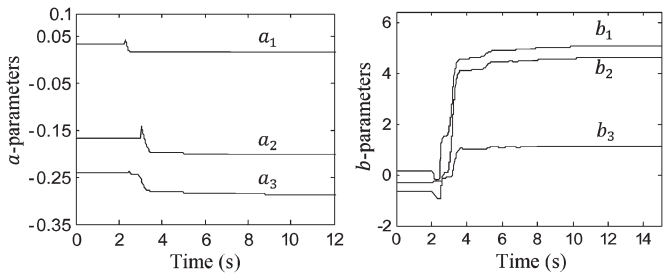

Fig. 14. Identified system parameters for a Type A disturbance.

A similar observation holds true when the test system is subjected to a Type C disturbance at the center of tie-line 7–8 with the damped inter-area power flow response shown in Fig. 18. However, the damping improvement by the ST controller is not significant when compared with other operating scenarios since the PI controllers were optimally tuned for this particular operating point. In another test, the tie-length is doubled from 250 km to 400 km and the performance of the overall UPFC damping model is tested for a disturbance of Type E and Type F. The corresponding damping responses are shown in Fig. 19.

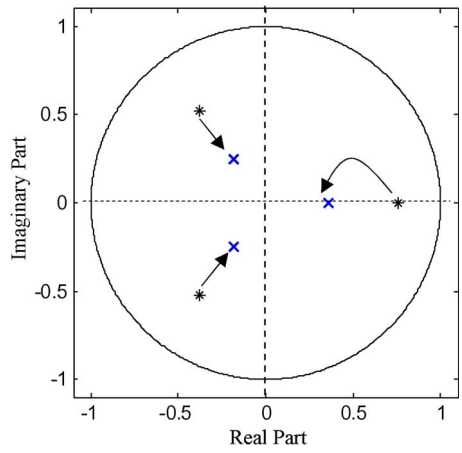

Fig. 15. Dynamic pole movement as a function of α for Type A disturbance.

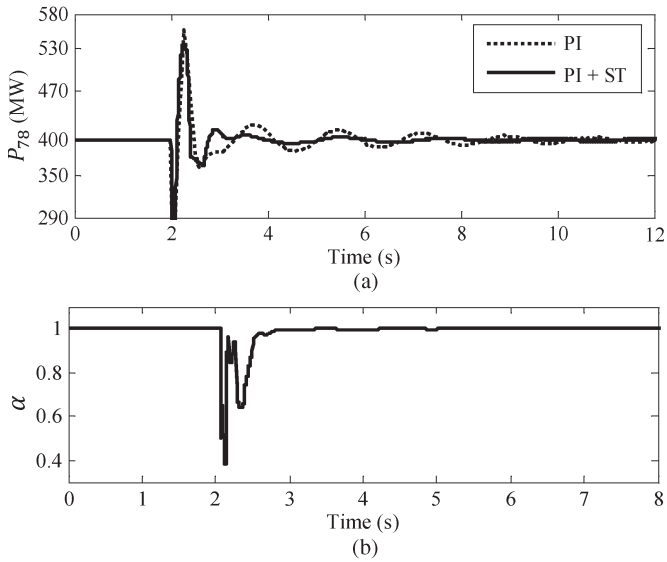

Fig. 16. Identified system parameters for a Type A disturbance.

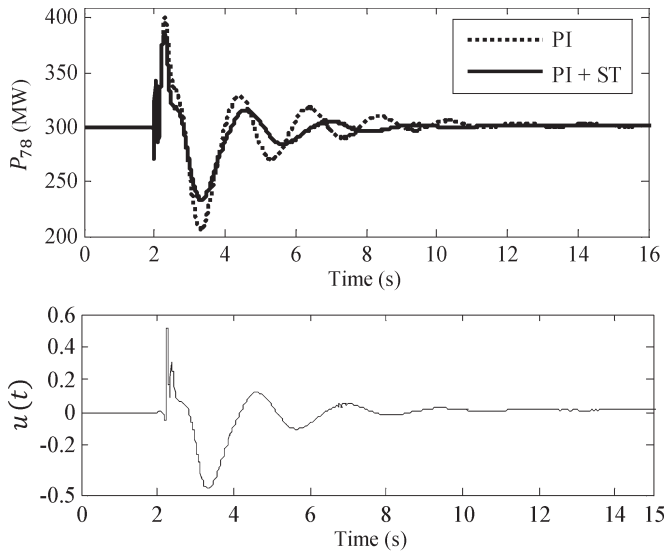

Fig. 17. System response to Type C disturbance.

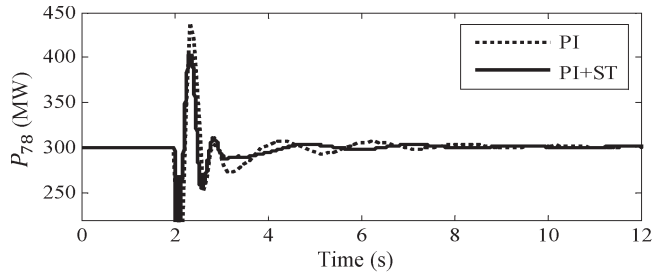

Fig. 18. Damped inter-area power oscillations for a Type D disturbance.

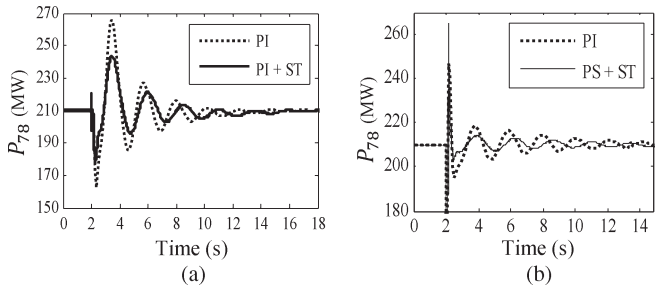

Fig. 19. Damped inter-area power oscillations. (a) System response to Type E; (b) system response to Type F.

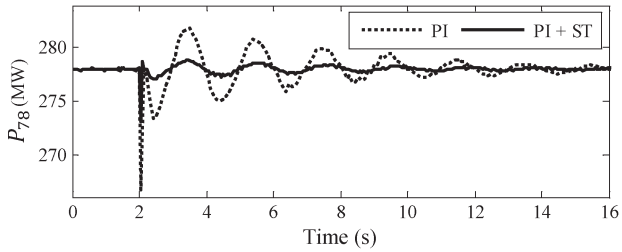

Fig. 20. Power damping comparison for Type G disturbance.

Furthermore, the positive impact of the add-on control scheme in damping inter-area oscillations was analyzed for operating condition IV, Type G fault. The corresponding power-flow oscillation after the application of fault is plotted in Fig. 20. It is clearly evident that the ST controller damps the oscillation within 10 s owing to its ability to adapt to different operating conditions without retuning.

B. Damping Improvement Assessment Using Prony Tool

The damping improvement shown in Table I is further investigated using Prony analysis tool. Table II shows the study results for the base case (without any damping controller) and the four test cases with the standalone-PI controllers and subsequently assisted with the proposed ST controller.

The Prony analysis tool is applied on the short circuit response of P_{78} to find the frequency and damping of the system's inter-area mode. It is clear from Table II that the inter-area oscillatory mode frequency lies between 0.43 and 0.58 Hz. Also, the corresponding damping ratio was found to be 2.4%–5.3% and being $\sim\leq 5\%$, is significantly under-damped. The overall damping improvement seen with PI controllers is typically between 6% and 10% whereas with the add-on ST controller is between 17% and 22%. However, the damping improvement by the ST controller observed for IInd operating

TABLE II
INTER-AREA OSCILLATION DAMPING CASE STUDIES

Operating Condition	No Damping Controller		With non-optimal PI controller		With PI+ST Controller		Overall Damping Improvement
	Frequency (Hz)	Damping Ratio (%)	Frequency (Hz)	Damping Ratio (%)	Frequency (Hz)	Damping Ratio (%)	
I	0.46	2.4	0.54	7.61	0.55	24	22%
II	0.44	5.1	0.57	9.85	0.58	14	9%
III	0.43	5.3	0.52	5.74	0.54	18	14%
IV	0.46	3.8	0.55	6.21	0.57	21	17%

TABLE III
MACHINE AND SYSTEM DATA

Generator data	$900\ MVA$, $20\ kV$, $r_a = 0.0025\ p.u.$, $x_1 = 0.2\ p.u.$, $x_d = 1.8\ p.u.$, $x_q = 1.7\ p.u.$, $x_d{}' = 0.3\ p.u.$, $x_q{}' = 0.55\ p.u.$, $x_d{}'' = 0.25\ p.u.$, $x_q{}'' = 0.25\ p.u.$,
	$T_{do}{}' = 8\ s$, $T_{do}{}'' = 0.03\ s$, $T_{qo}{}' = 0.4\ s$, $T_{qo}{}'' = 0.05\ s$, $H\ (G_1 = G_2 = 6.5)$, $H\ (G_3 = G_4 = 6.15)$
Transmission line data	$R_{line}\ (net) = 0.0529\ \Omega/km$, $X_{line}\ (net) = 0.529\ \Omega/km$
Exciter data	IEEE type ST1A exciter, $T_r = 0.01\ s$, $T_c = 1\ s$, $T_B = 10\ s$, $K_A = 50$, $V_{MAX} = 9\ p.u.$, $V_{MIN} = -9\ p.u.$
Steam governor data	GE mechanical-hydraulic controls, Droop, $R = 0.04\ p.u.$, Speed relay lag time constant, $T_1 = 0.1\ s$, Gate servo time constant, $T_3 = 0.25\ s$
Steam turbine data	IEEE type 2 thermal turbine, $K_1 = 0.0$, $K_2 = 0.25$, $K_3 = 0.25$, $K_4 = 0.5$, $K_5 = 0.0$, $K_1 = 0.0$, $K_7 = 0.0$, $K_8 = 0.0$, Steam chest time constant, $T_4 = 0.42\ s$, Re-heater time constant, $T_5 = 4.25\ s$, Re-heater/crossover time constant, $T_6 = 0.72\ s$
Transformer data	$900\ MVA, 20/230\ kV, x_t = 0.15\ p.u.$

condition is the lowest since the PI controllers were optimally tuned under this test. Overall, the proposed scheme provided significantly improved damping performance.

V. CONCLUSION

The add-on ST controller provided significant damping improvement for the inter-area mode as compared to the conventional PI-UPFC controllers. In addition, the proposed controller is capable of adapting to different system configurations and could be extended for any other type of FACTS device.

The use of constrained-RLS over the standard RLS identifier for online parameter identification ensured favorable control performance even during large disturbances.

The proposed ST control methodology is currently being applied for tuning of several FACTS (UPFC, STATCOM, SSSC) controllers in large power system configurations for achieving optimum power oscillation damping without affecting individual device performance. Wide area control signals taking into account issues such as communication delays [20] are being investigated. Experimental investigations using realtime hardware-in-the-loop simulations using a power system simulator would be reported in a future publication.

APPENDIX

See Tables III and IV.

TABLE IV
UPFC DESIGN PARAMETERS

GTO	ON resistance = $0.005\ \Omega$, OFF resistance = $1X10^{-8}\Omega$, Forward voltage drop = $0.0\ kV$, Forward break-over voltage = $1X10^5\ kV$, Reverse withstand voltage = $1X10^5\ kV$, PWM switching frequency, $f_c = 1980\ Hz$
Snubber circuit	Snubber resistance = $5000\ \Omega$, Snubber capacitance = $0.05\ \mu F$
Shunt coupling transformer	Three phase rating: $100\ MVA$, $Y-\Delta$, RMS line-line voltage = $230/20\ kV$, Leakage reactance = $0.1\ p.u.$, Air core reactance = $0.2\ p.u.$
Series coupling transformer	Single phase rating: $100\ MVA$, RMS line-line voltage = $13\ 0/20\ kV$, Leakage reactance = $0.1\ p.u.$, Air core reactance = $0.2\ p.u.$
DC link capacitance	$10\ mF$
UPFC PI parameters (tuned for Operating Condition I)	Shunt VSC DC link: $K_P = 0.2$, $T_I = 0.1\ s$ Shunt VSC AC bus: $K_P = 10$, $T_I = 0.01\ s$ Series VSC d-q control: $K_{Pd} = 0.08$, $T_{pd} = 0.44\ s$ $K_{Pq} = 0.05$, $T_{Iq} = 0.52\ s$

REFERENCES

[1] N. G. Hingorani and L. Gyugyi, *Understanding FACTS: Concepts and Technology of Flexible AC Transmission Systems*. New York, NY, USA: IEEE Press, 2000, pp. 315–319.

[2] K. M. Son and R. H. Lasseter, "A Newton-type current injection model of UPFC for studying low-frequency oscillations," *IEEE Trans. Power Del.*, vol. 19, no. 2, pp. 694–701, Apr. 2004.

[3] K. R. Padiyar and A. M. Kulkarni, "Control design and simulation of unified power flow controller," *IEEE Trans. Power Del.*, vol. 13, no. 4, pp. 1348–1354, Oct. 1998.

[4] B. S. Chen and Y. Y. Hsu, "A minimal harmonic controller for a STATCOM," *IEEE Trans. Ind. Electron.*, vol. 55, no. 2, pp. 655–664, Feb. 2008.

[5] P. Mitra and G. K. Venayagamoorthy, "An adaptive control strategy for DSTATCOM applications in an electric ship power system," *IEEE Trans. Power Electron.*, vol. 25, no. 1, pp. 95–104, Jan. 2010.

[6] S. Mohagheghi, Y. del Valle, G. K. Venayagamoorthy, and R. G. Harley, "A proportional-integral type adaptive critic design-based neuro controller for a static compensator in a multimachine power system," *IEEE Trans. Ind. Electron.*, vol. 54, no. 1, pp. 86–96, Feb. 2007.

[7] A. G. Loukianov, J. M. Cañedo, L. M. Fridman, and A. Soto-Cota, "High-order block sliding-mode controller for a synchronous generator with an exciter system," *IEEE Trans. Ind. Electron.*, vol. 58, no. 1, pp. 337–347, Jan. 2011.

[8] W. Qiao and R. G. Harley, "Indirect adaptive external neuro-control for a series capacitive reactance compensator based on a voltage source PWM converter in damping power oscillations," *IEEE Trans. Ind. Electron.*, vol. 54, no. 1, pp. 77–85, Feb. 2007.

[9] H. Ishibuchi and T. Nakaskima, "Improving the performance of fuzzy classifier systems for pattern classification problems with continuous attributes," *IEEE Trans. Ind. Electron.*, vol. 46, no. 6, pp. 1057–1068, Dec. 1999.

[10] X. Duan, H. Deng, and H. Li, "A saturation-based tuning method for fuzzy PID controller," *IEEE Trans. Ind. Electron.*, vol. 60, no. 11, pp. 5177–5185, Nov. 2013.

[11] C. Yan and G. K. Venayagamoorthy, "AIS-Based coordinated and adaptive control of generator excitation systems for an electric ship," *IEEE Trans. Ind. Electron.*, vol. 59, no. 8, pp. 3102–3112, Aug. 2012.

[12] M. Wei and T. Liu, "Design and implementation of an online tuning adaptive controller for synchronous reluctance motor drives," *IEEE Trans. Ind. Electron.*, vol. 60, no. 9, pp. 3644–3657, Sep. 2013.

[13] G. P. Chen, O. P. Malik, G. S. Hope, Y. H. Qin, and G. Y. Xu, "An adaptive power system stabilizer based on the self-optimizing pole shift control strategy," *IEEE Trans. Energy Convers.*, vol. 8, no. 4, pp. 639–645, Dec. 1993.

[14] R. Gokaraju and O. P. Malik, "Radial basis function identifier and pole-shifting controller for power system stabilizer application," *IEEE Trans. Energy Convers.*, vol. 19, no. 4, pp. 663–670, Dec. 2004.

[15] A. Domahidi, B. Chaudhuri, P. Korba, R. Majumder, and T. C. Green, "Self-tuning flexible ac transmission system controllers for power

oscillation damping: A case study in real time," *IET Gener. Transm. Distrib.*, vol. 3, no. 12, pp. 1079–1089, Dec. 2009.
[16] R. Sadikovic, P. Korba, and G. Andersson, "Self-tuning controller for damping power system oscillations with FACTS devices," in *Proc. IEEE Power Eng. Soc. Gen. Meet.*, 2007, pp. 1–6.
[17] K. Sen and M. L. Sen, *Introduction to FACTS Controller: Theory, Modeling, and Applications*. New York, NY, USA: IEEE Press, 2009, p. 298.
[18] K. J. Åström and B. Wittenmark, *Adaptive Control*, 2nd ed. New York, NY, USA: Dover, 2008.
[19] A. Gole, S. Filizadeh, R. Menzies, and P. Wilson, "Optimization enabled electromagnetic transient simulation," *IEEE Trans. Power Del.*, vol. 20, no. 1, pp. 512–518, Jan. 2005.
[20] R. Yang, G. Liu, P. Shi, C. Thomas, and M. V. Basin, "Predictive output feedback control for networked control systems," *IEEE Trans. Ind. Electron.*, vol. 61, no. 1, pp. 512–520, Jan. 2014.

Urvi Malhotra (S'09) received the B.E. degree in electronics engineering from the University of Mumbai, Mumbai, India, in 2008 and the M.Sc. degree in electrical engineering from the University of Saskatchewan, Saskatoon, Canada, in 2011.

Since May 2011, she has been working as a Network Management Engineer (EIT) at Saskatchewan Power Corporation in Regina, SK, Canada. Her research interests include flexible ac transmission systems and adaptive control.

Ramakrishna (Rama) Gokaraju (S'88–M'00) received the B.S. degree in electrical and electronics engineering from the Regional Engineering College, Trichy, India, in 1992 and the M.Sc. and Ph.D. degrees in electrical and computer engineering from the University of Calgary, Calgary, Canada, in June 1996 and May 2000, respectively.

During 1992–1994, he worked with Larsen & Toubro-ECC, India (Graduate Engineer), Regional Engineering College, Rourkela, India (Research Engineer), Indian Institute of Technology, Kanpur, India (Project Associate). During the period 2000 to 2002, he worked with the IBM Toronto Lab as a Staff Software Engineer. He joined the University of Saskatchewan in 2003 and is presently an Associate Professor. His current research work is in the area of real-time power systems simulations, adaptive control and smart grids.